Graefes Arch Clin Exp Ophthalmol (2014) 252:145–153
DOI 10.1007/s00417-013-2457-6

PATHOLOGY

Calibration of histological retina specimens after fixation in Margo's solution and paraffin embedding to in-vivo dimensions, using photography and optical coherence tomography

Stefan Koinzer · Sandra Bajorat · Carola Hesse · Amke Caliebe · Marco Bever · Ralf Brinkmann · Christoph Roecken · Johann Roider

Received: 13 March 2013 / Revised: 1 July 2013 / Accepted: 26 August 2013 / Published online: 14 September 2013

Abstract
Background The extent of retinal tissue deformation by histological processing needs to be separately measured for every workup protocol. This work presents a simple approach for its quantitative assessment, and shows lateral and axial scaling factors for a common protocol. We calibrated histological measurements by in-vivo photographic and optical coherence tomographic (OCT) measurements, using retinal photocoagulation lesions as calibration markers.
Methods We evaluated four rabbit eyes that were examined histologically after fixation in Margo's solution (1 % paraformaldehyde:1.25 % glutaraldehyde), isopropanol dehydration, paraffin embedding and hematoxylin and eosin staining. Distances between 51 pairs of laser lesions were compared in photographs and on histological slides. Retinal thickness measurements were performed at 15 anatomically defined sites in these eyes, and related to anatomically matched OCT thickness measurements of six different rabbit eyes.
Results We found that the ratio of histological over photographic lesion distances was 1.17 (95 % CI 1.13–1.22), indicating 17 % lateral retinal stretching or expansion by the processing. Thickness measurements in histology were 65.6 % of the in-vivo thickness as measured in OCT, indicating 1/3 axial tissue compression or shrinkage.
Conclusions We provide an analysis of retinal tissue deformation after fixation in Margo's solution and paraffin embedding. In spite of protocol optimization for reduced tissue deformation, the workup caused 1/3 axial compression/shrinkage and 17 % lateral elongation, which was unexpected. We show a simple way how to calibrate retina specimens by

This research was conducted in a collaborative project which was supported by the German Federal Ministry of Education and Research (BMBF).The authors have full control of all primary data, and they agree to allow Graefe's Archive for Clinical and Experimental Ophthalmology to review their data upon request.

S. Koinzer (✉) · S. Bajorat · C. Hesse · J. Roider
Department of Ophthalmology, University Hospital of Schleswig–Holstein, Campus Kiel, House 25, Arnold-Heller-Str. 3, 24105 Kiel, Germany
e-mail: koinzer@auge.uni-kiel.de

S. Bajorat
e-mail: sandra.thuete@gmx.de

C. Hesse
e-mail: carola.hesse@gmx.net

J. Roider
e-mail: roider@auge.uni-kiel.de

A. Caliebe
Institute of Medical Informatics and Statistics, University Hospital of Schleswig–Holstein, Campus Kiel, House 31, Arnold-Heller-Str. 3, 24105 Kiel, Germany
e-mail: caliebe@medinfo.uni-kiel.de

M. Bever · R. Brinkmann
Medical Laser Center Lübeck GmbH, Peter-Monnik-Weg 4, 23562 Lübeck, Germany

M. Bever
e-mail: m.bever@web.de

R. Brinkmann
e-mail: brinkmann@mll.uni-luebeck.de

fundus photography and OCT, two methods that are readily available to most ophthalmologists. Our findings underline the necessity to calibrate specimens prior to morphometry.

Keywords Morphometry · Histology · Deformation · Artifact · OCT · Optical coherence tomography · Retina · Rabbit

Introduction

Tissue samples are subject to significant deformation through histological processing, which may introduce measurement errors of up to 300 % if the specimens are not properly calibrated [1]. In the case of larger specimens, calibration is feasible to macroscopic measurements before processing. Very thin and fragile tissues such as retina, however, are not eligible for macroscopic measurements. The globe shape of the eye enhances the difficulties in such measurements. Consequently, calibration by in-situ measurements would be advantageous. We used fundus color photography for lateral and optical coherence tomography (OCT) for axial calibration of histological sections.

The retina is approximately 200 μm thick, depending on the species and the anatomical origin (Koinzer et al., in press in Acta Ophthalmologica). It contains primarily neuronal tissue. Under in-vivo conditions, three forces—osmotic pressure, active fluid shift through the underlying retinal pigment epithelium (RPE), and hydrostatic pressure—keep it attached [2]. Post mortem, the bulk of these forces, which depend on active metabolic processes, breaks down, which puts the retina at a high risk of detachment and destruction during the histological processing. Margo and Lee have systematically examined corneal clarity, tissue deformation, retinal attachment, and tissue preservation after whole-eye fixation through different fixatives, and suggested a mixture of 1 % of phosphate-buffered formaldehyde and 1.25 % glutaraldehyde (Margo's solution) [3]. To date, this fixative is widely used in ophthalmic pathology in cases where tissue samples are too large for plastic embedding.

In this rabbit study, we applied in-vivo color fundus photography for length calibration and optical coherence tomography (OCT) for thickness calibration of our specimens after they had been fixated in Margo's solution and processed for histology. Moderately intense laser lesions served as landmarks on the retina that could be localized in-vivo and in specimens as well, but did not attach the retina.

Material and methods

Our study had two independent arms, one including four eyes of two rabbits that underwent fundus photography and histological processing, the other one including six eyes of three rabbits that were examined by OCT. Fundus photographies and histological images originated from identical animals, while thickness calibration was done by statistical correlation of anatomically matched OCT and histological measurements from different animals.

Animal treatment

We placed grids of 150–300 moderate laser burns on the retinas of chinchilla grey rabbits by conventional retinal photocoagulation, producing grey to white funduscopic lesions (Fig. 1). The animals were treated under general and local anesthesia, with dilated pupils. Laser irradiation was delivered through a modified Mainster focal grid laser contact lens which had been fitted onto the eye with methylcellulose gel (2 %). We performed photocoagulation with a slightly modified 532 nm continuous wave laser system (VISULAS VITE, Carl Zeiss Meditec AG, Jena, Germany). The irradiation diameter was 133 μm on the fundus. Powers—and the resulting lesion intensities—were variable, and exposure times were 200 ms, or automatically controlled as published elsewhere [4, 5].

The rabbits were maintained in animal units at the University Medical Center of Schleswig–Holstein, and all animal experiments have been carried out according to the German law for protection of animals and approved by the Ministry of Energy Transition, Agriculture, the Environment, and Rural Areas of Schleswig–Holstein, Kiel, Germany (application no.

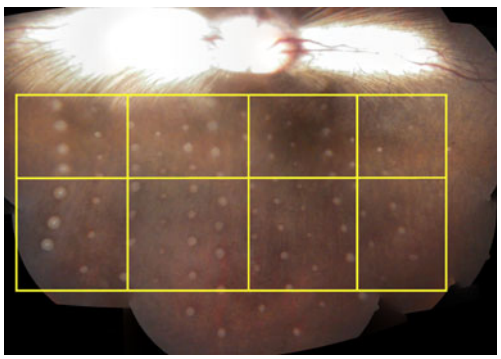

Fig. 1 Panoramic view of a rabbit fundus. Single photographs were digitally assembled by Hugin-software, ver. 2010.2.0 (www.hugin.sourceforge.net). At the upper edge, the optic papilla (middle), the big retinal vessels, and the medullary ray are displayed. The visual streak is located underneath the papilla and medullary ray. The natural appearance of a rabbit fundus is reddish to brown, depending on the pigment density in the underlying retinal pigment epithelium and choroid. Grey to white round spots with variable diameters are photocoagulation burns of variable intensities. *Yellow lines* show the rectangular pattern that we used for standardization of thickness measurement location. The *horizontal lines* run parallel to the medullary ray, and 1 mm, 3 mm, and 6 mm below it, and the *vertical lines* run through the optic papilla, the ends of the medullary ray and halfway in between. We measured the retinal thickness at the intersections of these lines ($n=15$) in each eye

V312-7234.121-11). The experiments followed the "Principles of laboratory animal care" (NIH publication No. 85–23, revised 1985), the OPRR Public Health Service Policy on the Humane Care and Use of Laboratory Animals (revised 1986), and the U.S. Animal Welfare Act, as amended.

Histological processing

Six hundred and forty-five photocoagulation lesions were applied to four eyes of two rabbits that underwent histological examination. Fundus photographies were recorded 1 h after each photocoagulation treatment with a Zeiss VISUCAM (Carl Zeiss Meditec AG, Jena, Germany). After enucleation, we fixated the eyes in Margo's solution for 2 h, removed the anterior segments, and continued fixation in Margo's solution for 1–2 days at room temperature. The area of interest was cut out of a retina–choroid–sclera preparation, marked with color, dehydrated in increasing isopropanol concentrations at room temperature (3×70 % for 24 h, 1×80 % for 8 h, 1×90 % over night, 3×100 % for 8 h), infiltrated and embedded in paraffin at its melting temperature of 56 °C (1 : 1 isopropanol:paraffin mixture for 90 min, 3×100 % paraffin for 24 h, then blocked in paraffin and cooled). Then we cut the cooled block (~0 °C) slowly into 5 μm slices at 50 μm distances and stained the sections with hematoxylin and eosin. Stronger photocoagulation lesions, color marks, the optic nerve, and the spatial relation of lesions were used to identify laser lesions within the specimens and correlate them to fundus photographies. We localized 508 of 645 lesions in histological sections. One hundred and thirty-seven lesions could not be localized because the irradiation power had been too low, because lesions had healed or because of tissue destruction during the processing.

Fundus image calibration

In order to assess the scale of digital fundus photographies, we had applied calibration lesions with an irradiated fundus diameter of 333 μm in preliminary experiments on nine rabbits. The lesions had been applied adjacent to each other, producing center-to-center distances that lay 1 lesion diameter apart. Five lesions were applied in a cross-pattern as shown in Fig. 2, allowing to measure the distance of 2 lesion diameters in x- and y-direction each. We found a pixel-to-micrometer ratio of 9.5±0.7 μm/pixel, equally on horizontal and vertical scales and comparable scalings, independently of the animal used.

Retinal length calibration

Lesion diameters could not be used for measurement calibration, because lesions are not sharply displayed. To calibrate retinal length deformation, we identified pairs of photocoagulation lesions that were visible in one histological section and measured center-to-center distances. These were correlated to the distances of the same lesion pairs on photographic fundus images.

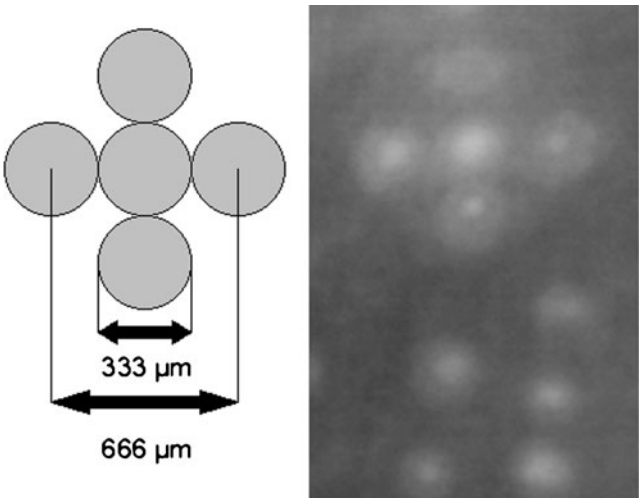

Fig. 2 Illustration of photographic image calibration. Schematic drawing on the left, photographic image on the right. We applied five laser lesions in a cross-pattern, with each lesion having a diameter of 333 μm on the fundus. We used center-to-center distances for length measurements, because the outline of a lesion is not sharply displayed (*right*), and because the size of the retinal whitening depends on the burn intensity. The cross-pattern of lesions facilitated 2-dimensional photo calibration by a double center-to-center distance of 666 μm in each axis

A total of 51 lesion pairs were identified and measured in histological sections and on fundus images as well. They were taken from all four rabbit eyes (see Table 1).

Retinal thickness calibration

The retinal thickness varies according to its anatomical location. In the rabbit eye, the optic nerve enters the eye above the optical center. To the left and right of the optic papilla, a horizontally extended area of myelinated nerve fibres called "medullary ray" appears white in the fundus image (Fig. 1). Here, the nerve fibre layer of the inner retina is particularly thick. Below the medullary ray lies an area of maximal retinal sensitivity which is called "visual streak", and where the retina

Table 1 Distance ratio of identical laser lesion pairs in histological slides and fundus photographies (mean ± standard deviation). Data are displayed for each of the four study eyes separately. Below, the values for all four eyes and the 95 % confidence interval (CI) are given

Rabbit no.	Eye	Ratio histology/photo (mean±SD)	*N*
1	1	1.18±0.07	13
	2	1.16±0.19	16
2	1	1.17±0.16	14
	2	1.17±0.22	8
	All	1.17±0.16 (95 % CI : 1.13–1.22)	51

is thickened. Aside from the visual streak, retinal thickness decreases with increasing eccentricity, i.e., increasing distance from the optic papilla [6].

As laser-treated retina deforms differently than healthy retina (Koinzer at al., in press in Acta Ophthalmologica), we chose spots of healthy retina for thickness measurements. In order to compensate for anatomical thickness variations, we measured thicknesses at the corners of a standardized rectangular pattern on the fundus as shown in Figs. 1 and 3. The rectangles were separated by vertical lines through the optic papilla, the left and right end of the medullary ray, and halfway between these lines. Horizontal borders of the rectangles ran parallel to the medullary ray at 1 mm, 3 mm, and 6 mm distance below it.

Figure 3 shows a representative OCT image that we used for in-vivo thickness measurements. We applied a spectral-domain OCT (HRA + OCT Spectralis®, Heidelberg Engineering, Heidelberg, Germany) and scanned the area of interest at 30-μm steps. Every sectional image was obtained by averaging of 20 sweeps to optimize image quality. Along with the OCT sectional images, the OCT machine records a calibrated infrared (IR) image of the ocular fundus that serves as a locator. We used the IR image to find and mark the corners of the rectangular pattern as indicated in Fig. 3. The retinal thickness was measured with the proprietary software of the OCT machine. We used sectional images that were displayed in the 1:1 μm mode and magnified 8-fold for the measurement.

In histological specimens, the optic papilla/optic nerve and end of the medullary ray were used to find the horizontal positions for thickness measurements, i.e., the correct slides in a consecutive series. The distances of 1, 3, and 6 mm below the medullary ray were measured in the specimens, and the retinal thickness determined from the innermost ganglion layer to the outermost retinal pigment epithelium (RPE) layer.

Statistical analyses

We calculated means, standard deviations, and the 95 % confidence interval of the mean of the histological/photographic distance ratios. The influence of the individual eye on this ratio was analysed by a one-way ANOVA.

For the analysis of retinal thickness, the influence of location (lateral and vertical eccentricity) was tested by an ANOVA analysis with eye as an additional random factor, followed by a Scheffé post-hoc analysis. An ANOVA for repeated measurements was applied to test for the measurement method (OCT

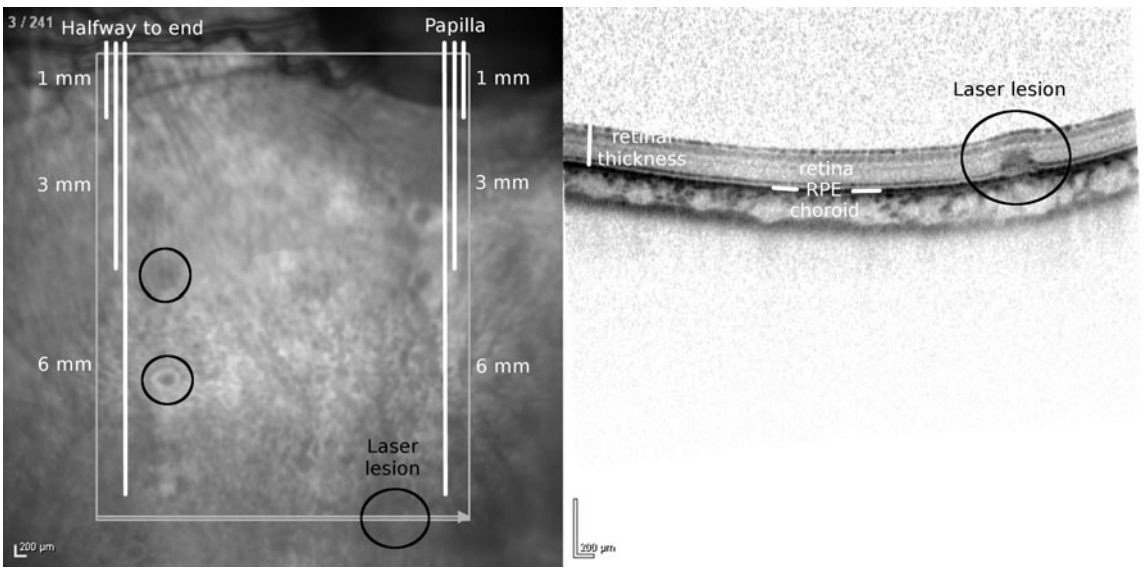

Fig. 3 An image generated by our spectral-domain OCT device. The *left* shows an infrared image (IR) of the fundus, with the optic papilla in the *upper right corner* and the right part of the medullary ray and the large vessels at the *upper left border*. The *right part of the figure* shows one individual sectional OCT image. Note that the scale of the sectional image is 4 times greater in vertical than in horizontal direction due to differential resolutions of the device ("1:1 pixel" mode), giving the image a distorted appearance compared to histology slides. A *light gray box* in the left image shows the area which was covered by the OCT scans. The *light gray arrow* at the lower border demarcates the position and direction of the actual scan shown on the right, and the *small number in the very left upper corner* indicates that this is section no. 3 in a series of 241. We scanned the area at 30 μm steps. *Black circles* indicate some of the laser lesions. The lower right lesion in the IR image is the same as that displayed in the section. *White annotations* indicate how retina thickness measurements were performed. In the IR image, two horizontal positions of measurement are visible (optic papilla and halfway of papilla to right end of medullary ray). *White lines* show how the locations for retinal thickness measurements were found below these two horizontal positions at 1, 3, and 6 mm distances from the medullary ray. In the sectional image, the choroid, retina, and retinal pigment epithelium (RPE) are labelled. The RPE is the outermost cellular layer of the retina. A *vertical white line* shows the distance we assessed as retinal thickness, including the ganglion cell and nerve fibre layers as inner limit and the RPE as outer limit. Even though the IR image appears a little blurred, distances in OCT sections are clearly recognizable

vs histology; between subjects factor) as well as location (two within subjects factors) with and without interaction.

P-values below 0.05 were considered statistically significant. All statistical analyses were carried out with SPSS software, version 20.

Results

Length deformation in histological slides (Table 1)

The ratio of histological lesion pair distances over photographical lesion pair distances of identical pairs is given in Table 1 for each rabbit eye separately and for all eyes. The length ratios showed good accordance between the eyes, and were not significantly different ($p=0.99$). The overall mean ratio was 1.17 (range 0.81–1.55), with a 95 % confidence interval of 1.13–1.22. Obviously, the retina was stretched or expanded laterally by about 17 % on histological slides.

Influence of individual eye and anatomical location on retinal thickness (Figs. 4 and 5)

The influence of the eye side (right vs left) on the retinal thickness was neither significant in OCT ($p=0.56$) nor in histology ($p=0.27$). The retinal thickness was significantly different in different eyes ($p<0.001$). Two homogenous subgroups were differentiated by the Scheffé analysis, one comprising three eyes with histological measurements (Fig. 4), the other one all six eyes with OCT measurements. The remaining eye ("Histo1") was not statistically attributable to either group.

The influence of lateral eccentricity on retinal thickness measurements (optic papilla, halfway to end of medullary ray, and end of medullary ray) was significant neither in OCT ($p=0.38$) nor in histology ($p=0.94$), nor in the overall evaluation ($p=0.86$, Fig. 5a). The influence of vertical eccentricity was significant in OCT ($p<0.001$), in histological measurements ($p=0.01$), and in the overall evaluation ($p<0.001$, Fig. 5b). The Scheffé post-hoc analysis showed that the subgroups 1 and 3 mm below the medullary ray were homogenous, but the measurements 6 mm below the medullary ray were significantly different from the other groups ($p<0.001$).

In the multiple analysis with both lateral and vertical eccentricity as influence variables, only vertical eccentricity ($p<0.001$) showed a significant effect on the retinal thickness.

Comparison of retinal thickness in OCT images and histological slides

An ANOVA analysis with repeated measurements showed that the retinal thicknesses differed highly significantly in OCT images (mean±SD, 160.7±13.3 μm) and in histology (105.4±17.3 μm, $p<0.001$). The ratio of mean values was 105.4 / 160.7=65.6 %, indicating retinal shrinkage by 1/3 by the histological processing. No significant interaction between

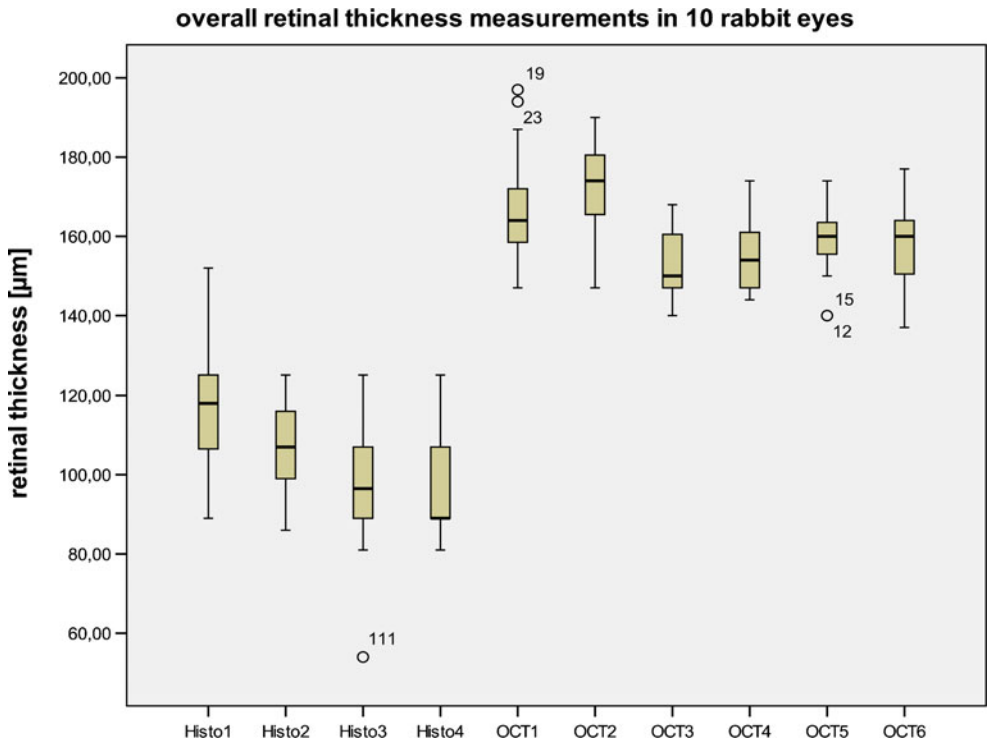

Fig. 4 Box plots of retinal thickness measurements in all ten rabbit eyes of the study

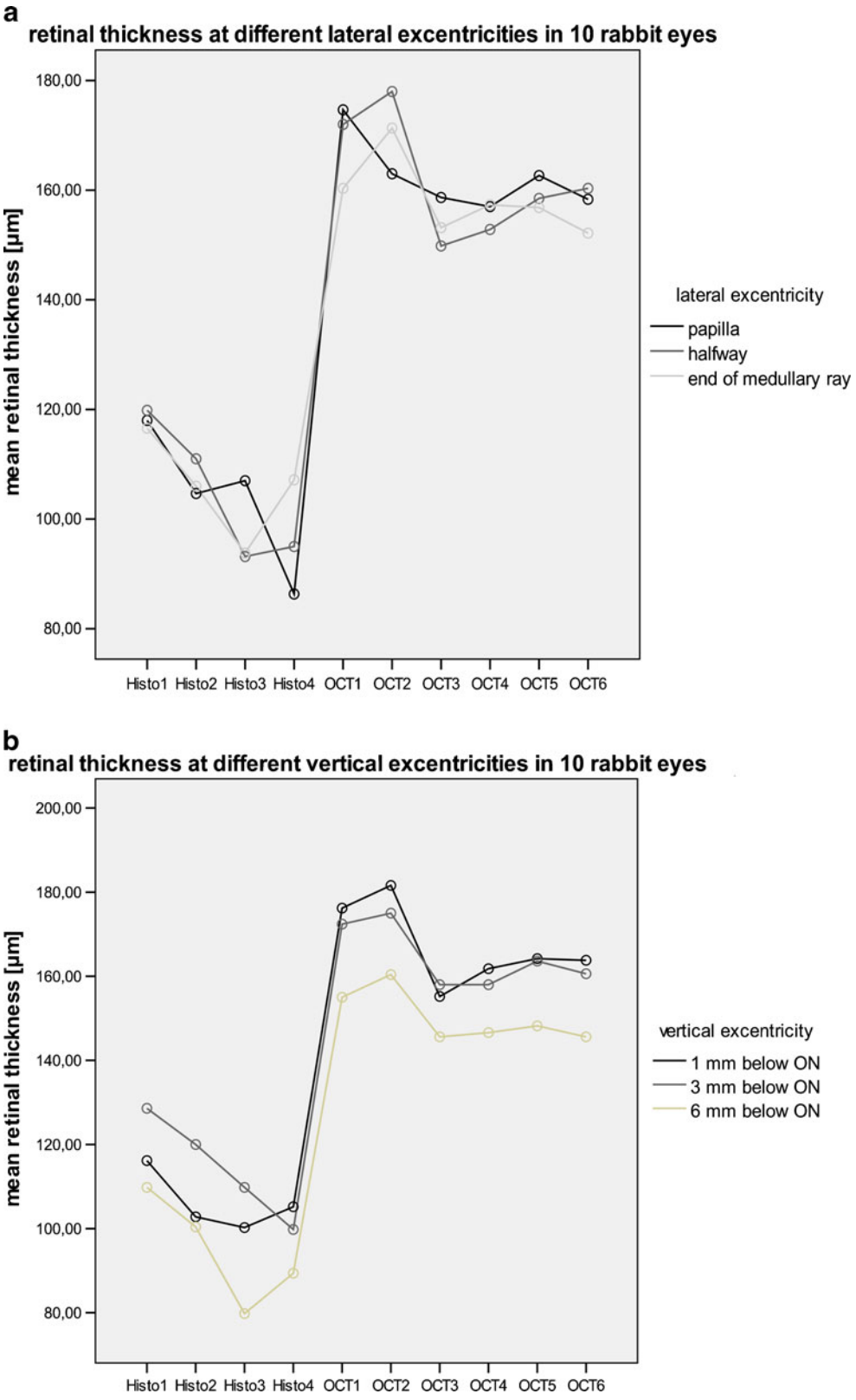

Fig. 5 **a** and **b**: Influence of anatomical location on the retinal thickness measurement in OCT images. **a** Mean values of retinal thickness measurements at different lateral eccentricities (optic papilla [*black*], end of medullary ray [*light grey*], middle in between both [*intermediate grey*]). **b** Mean values of retinal thickness measurements at different vertical eccentricities (1 mm [*black*], 3 mm [*intermediate grey*] or 6 mm [*light grey*] below the medullary ray). *ON*: optic nerve

vertical eccentricity and the method of measurement was found.

A digital photographic simulation of the retinal tissue deformation is shown in Fig. 6.

Discussion

In this study, we investigated retinal tissue deformation after a common histological workup protocol that uses Margo's

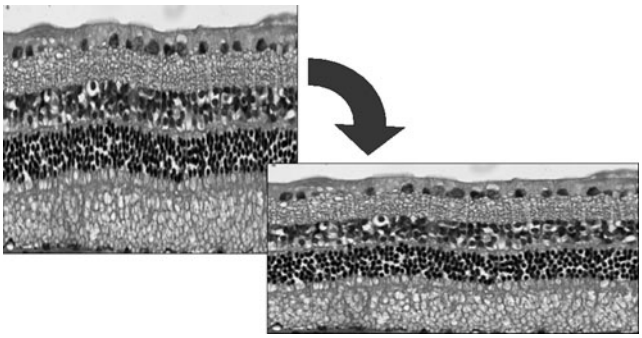

Fig. 6 Dimensions of a piece of retina prior to and after histological processing are digitally simulated, with original dimensions being simulated in the *top left image* and histological dimensions in the *lower right image*. By histological processing according to the protocol we used, the retina shrinks or is compressed axially by about 1/3 and expands or is stretched laterally by about 17 %

solution as fixative for paraffin embedding. In-vivo OCT images served as retinal thickness reference. Thickness calibration was performed on 15 measurements each from four eyes for histology (60 measurements), and from six eyes for OCT (90 measurements). For retinal length correction, we used top view photographs of the tissue that we calibrated in relation to laser lesions of defined center-to-center-distances. We measured and correlated 51 distances of laser lesion pairs in photographies and on histological slides. Our analysis revealed about 17 % lateral expansion or stretching of the retina and about 1/3 vertical shrinkage or compression, respectively.

The retina is dominated by neuronal tissue, and contains about 84 % water [7] and little collagen. Due to its high protein content, it is better fixated with glutaraldehyde than formalin. The underlying choroid is dominated by vascular tissue, while the sclera is dominated by collagen fibres (50–75 %) and contains about 68 % water [8]. It is reasonable to assume that the underlying tissues react to processing chemicals differently than retina. This implicates that a retinal pathology may be located alongside the corresponding choroidal location in a histological specimen, and in fact a lateral shift of slightly detached retina or lateral traction of attached retina may be frequently observed at photocoagulation lesions [9, 10]. Histological analyses of chorio-retinal interactions should consider that.

Tissue deformation through histological processing has been thoroughly examined over decades in numerous tissue types such as liver [11], kidney [12]; lung [13], and others. Recently, differential tissue shrinkage in the z-axis has been discovered in the context of 3-dimensional particle counting by the optical dissector, and two extensive studies have proposed feasible methods for differential z-axis calibration [14, 15]. The method relies on particle count percentiles in different tissue layers, and is applicable to thick sections of homogenous tissue, but not on thin tissue layers of variable differentiations. If thin, layered structures are to be calibrated, OCT is a useful tool, which is also applicable and commercially available for ex-vivo microscopy [16, 17], and which is increasingly applied in other medical specializations than ophthalmology such as dermatology [18], cardiology [19], and others.

Retinal OCT-to-histological layer analyses have been done on plastic embedded sections by Knott et al. [20], where the retinal thickness was merely the same in OCT and histology. In that study on murine eyes, the optic nerve width was used to calibrate OCT images according to histological measurements, which might be an explanation for the high agreement of both measurements. Another study compared retinal thicknesses in primate eyes after plastic embedding, and found about 1/3 axial shrinkage, which agrees with our findings from paraffin histology [21]. A recent study by Curcio et al. compared retinal OCT and histology of the human macula [22]. They used a modified workup protocol for electron microscopy, which led to a retinal thickness reduction as well. The authors calculated a median tissue volume decrease of 14.5 % overall, and of 29 % in the fovea, through the processing. Others found volume changes by as much as 40–50 % through the processing [21, 23].

In contrast to the cited studies, we calibrated specimens for lateral deformation as well. It has been shown before that axial and lateral deformation do not necessarily correlate [24]. Using photocoagulation lesions, we found 17 % lateral elongation of the retina. It is unlikely that the laser lesions themselves influenced this value significantly. Strong lesions may induce fibrous scars that span Bruch's membrane. In these cases, photocoagulation attaches the retina to the underlying tissue ("retinopexy"). In lesions where Bruch's membrane remains intact, such as those applied in our study, however, the retina will rather split or detach completely and move sideways, as may be observed in many histological images from photocoagulation lesions [9, 10].

Tissue deformation occurs during fixation — collagen fibres swell in low formaldehyde concentrations — and depends on the fixation agent and its osmolality. Higher fixation agent osmolality causes increasing tissue shrinkage. To minimize these effects, we used the fixative suggested by Margo and Lee, which minimized ocular tissue deformation [3]. Furthermore, dehydration tends to cause tissue shrinkage, and embedding and cutting cause further deformation. Cutting may indeed cause compression in the cutting direction, and this effect increases with decreasing section thickness [24]. The correction factor for this compression was in the order of 0.9 to 0.952 in lung tissue, and is neglected by some authors [1]. In our processing protocol, the blade ran from the retinal side toward the sclera in order to prevent artificial retinal detachment, and the shrinkage (or compression) factor was 0.656. The study design does not make it possible to differentiate compression by the blade from shrinkage by processing chemicals. In order to minimize mechanical compression,

we cooled the paraffin block to 0 °C during cutting. Plastic embedding is thought to prevent compression even more effectively, but has allowed the same amount of compression or shrinkage that we found [21].

The magnification factor that we applied to calculate the laser beam diameter in rabbit eyes (0.66) represents a possible source of error. The rabbit eye has a total refractive power of 100 D, vs 60 D in humans, and the axial length in female pigmented adult rabbits is 15.5 mm, vs 24.5 mm in humans [27, 28]. The factor of 0.66 was based on our own calculations, and is confirmed by other authors as well [25, 26]. It includes laser beam diminuation by the optics of the rabbit eye and magnification by the contact lens (×1.05). A selected laser beam diameter of 200 μm resulted in an irradiated retina diamter of 133 μm, and a selected 500 μm beam resulted in an irradiated diameter of 333 μm. Alternatively, instead of calibrating photographic in-vivo images, direct (photographic) measurements could have been conducted on rabbit eyes after enucleation and removal of the anterior segments. This approach would have introduced different sources of error such as fixation, which we began prior to opening the globes, and measurement on a flat photographic image of a spherical structure. We assume that the in-vivo measurements that we performed on calibrated images come closer to reality.

It is a limitation of our study design that we assessed OCT and histological retinal thicknesses in different animals. Although measurement of both in the same animal may be advantageous, our statistical post-hoc analysis revealed that the retinal thickness was only significantly influenced by the vertical eccentricity (significantly thinner 6 mm below the medullary ray) and by the assessment method — OCT vs histology.

In summary, we provide an analysis of retinal tissue deformation by a commonly used histological workup protocol, which uses Margo's solution as fixative. In spite of its optimization for reduced tissue deformation, the workup caused 1/3 axial compression/shrinkage and 17 % lateral stretching/expansion, which was unexpected. As the actual values depend on many factors and cannot be transferred to specimens from other laboratories, we show a simple way how to calibrate retina specimens by fundus photography and OCT, two methods that are readily available to most ophthalmologists. Our findings underline the necessity to calibrate specimens prior to morphometry.

Acknowledgements The authors declare that they have no conflict of interest.

The data were presented at the following conference:

• Annual meeting of the German-speaking Ophthalmopathologists, Erlangen, Germany; October 26/27, 2012.

The authors gratefully acknowledge grant support for this collaborative research project by the German Ministry of Education and Research (BMBF) according to the Innovation Award for Advancing Medical Technology 2006, grant #01EZ0734 (Dept. of Ophthalmology, University hospital of Schleswig-Holstein, Campus Kiel), #01EZ0732 (Medical Laser Center Lübeck), #01EZ0733 (Institute of Biomedical Optics Lübeck) and #01EZ0735 (Carl Zeiss Meditec AG).

Technical assistance by Monika Marquardt, Serap Luick, and Barbara Fluke is also gratefully acknowledged.

References

1. Oberholzer M (1983) Morphometrie in der klinischen Pathologie. Allgemeine Grundlagen. Springer, Berlin Heidelberg New York
2. Quintyn JC, Brasseur G (2004) Subretinal fluid in primary rhegmatogenous retinal detachment: physiopathology and composition. Surv Ophthalmol 49:96–108
3. Margo CE, Lee A (1995) Fixation of whole eyes: the role of fixative osmolarity in the production of tissue artifact. Graefes Arch Clin Exp Ophthalmol 233:366–370
4. Koinzer S, Schlott K, Ptaszynski L, Bever M, Kleemann S, Saeger M, Baade A, Caliebe A, Miura Y, Birngruber R, Brinkmann R, Roider J (2012) Temperature-controlled retinal photocoagulation — a step toward automated laser treatment. Invest Ophthalmol Vis Sci 53:3605–3614
5. Schlott K, Koinzer S, Ptaszynski L, Bever M, Baade A, Roider J, Birngruber R, Brinkmann R (2012) Automatic temperature-controlled retinal photocoagulation. J Biomed Opt 17:061223
6. Prince JH (1964) The rabbit in eye research. Charles Thomas, Springfield
7. Stefánsson E, Wilson CA, Lightman SL, Kuwabara T, Palestine AG, Wagner HG (1987) Quantitative measurements of retinal edema by specific gravity determinations. Invest Ophthalmol Vis Sci 28:1281–1289
8. Watson PG, Young RD (2004) Scleral structure, organisation and disease. A review. Exp Eye Res 78:609–623
9. Yu AK, Merrill KD, Truong SN, Forward KM, Morse LS, Telander DG (2013) The comparative histologic effects of subthreshold 532 nm and 810 nm diode micropulse laser on the retina. Invest Ophthalmol Vis Sci 54(3):2216–2224. doi:10.1167/iovs.12-11382
10. Hoerster R, Muether PS, Vierkotten S, Schröder S, Kirchhof B, Fauser S (2012) In-vivo and ex-vivo characterization of laser-induced choroidal neovascularization variability in mice. Graefes Arch Clin Exp Ophthalmol 250:1579–1586
11. Bahr GF, Bloom G, Friberg U (1957) Volume changes of tissues in physiological fluids during fixation in osmium tetroxide or formaldehyde and during subsequent treatment. Exp Cell Res 12:342–355
12. Davies DJ, Brewer DB, Hardwicke J (1978) Urinary proteins and glomerular morphometry in protein overload proteinuria. Lab Invest 38:232–243
13. Weibel ER (1979) Morphometry of the human lung: the state of the art after two decades. Bull Eur Physiopathol Respir 15:999–1013
14. Hatton WJ, von Bartheld CS (1999) Analysis of cell death in the trochlear nucleus of the chick embryo: calibration of the optical disector counting method reveals systematic bias. J Comp Neurol 409:169–186
15. Gardella D, Hatton WJ, Rind HB, Rosen GD, von Bartheld CS (2003) Differential tissue shrinkage and compression in the z-axis: implications for optical disector counting in vibratome-, plastic- and cryosections. J Neurosci Meth 124:45–59
16. Li Q, Onozato ML, Andrews PM, Chen CW, Paek A, Naphas R, Yuan S, Jiang J, Cable A, Chen Y (2009) Automated quantification of microstructural dimensions of the human kidney using optical coherence tomography (OCT). Opt Express 17:16000–16016
17. Mujat M, Greco K, Galbally-Kinney KL, Hammer DX, Ferguson RD, Iftimia N, Mulhall P, Sharma P, Pikal MJ, Kessler WJ (2012)

Optical coherence tomography-based freeze-drying microscopy. Biomed Opt Express 3:55–63
18. Gambichler T, Jaedicke V, Terras S (2011) Optical coherence tomography in dermatology: technical and clinical aspects. Arch Dermatol Res 303:457–473
19. Regar E, Ligthart J, Bruining N, van Soest G (2011) The diagnostic value of intracoronary optical coherence tomography. Herz 36:417–429
20. Knott EJ, Sheets KG, Zhou Y, Gordon WC, Bazan NG (2011) Spatial correlation of mouse photoreceptor–RPE thickness between SD-OCT and histology. Exp Eye Res 92:155–160
21. Anger EM, Unterhuber A, Hermann B, Sattmann H, Schubert C, Morgan JE, Cowey A, Ahnelt PK, Drexler W (2004) Ultrahigh resolution optical coherence tomography of the monkey fovea. Identification of retinal sublayers by correlation with semithin histology sections. Exp Eye Res 78:1117–1125
22. Curcio CA, Messinger JD, Sloan KR, Mitra A, McGwin G, Spaide RF (2011) Human chorioretinal layer thicknesses measured in macula-wide, high-resolution histologic sections. Invest Ophthalmol Vis Sci 52:3943–3954
23. Abbott CJ, McBrien NA, Grünert U, Pianta MJ (2009) Relationship of the optical coherence tomography signal to underlying retinal histology in the tree shrew (Tupaia belangeri). Invest Ophthalmol Vis Sci 50:414–423
24. Baur R (1969) Error correction by sterologic measuring on human placenta. 2. Cutting compression. Experientia 25:1173
25. Paulus YM, Jain A, Gariano RF, Stanzel BV, Marmor M, Blumenkranz MS, Palanker D (2008) Healing of retinal photocoagulation lesions. Invest Ophthalmol Vis Sci 49:5540–5545
26. Birngruber R (1991) Choroidal circulation and heat convection at the fundus of the eye. In: Wolbarsht ML (ed) Laser applications in medicine and biology. Plenum Press, New York, pp 277–358
27. Verolino M, Nastri G, Sellitti L, Costagliola C (1999) Axial length increase in lid-sutured rabbits. Surv Ophthalmol 44(Suppl 1):103–108
28. Park HS, Kim JY, Shin JP, Choi YJ, Kim SY (2005) Effect of experimental scleral shortening on axial length of the rabbit eye. Korean J Ophthalmol 19:101–205